

as does zinc, but aluminum does not afford as many carbonyls. Lastly, zinc sputtering causes both the main peak to broaden and oxidizes graphene to produce carbonyl groups. The oxidation can be explained by reaction of the carbon radicals at the newly formed defect sites with traces of oxygen present in the sputtering chamber (5×10^{-5} torr) or upon subsequent exposure to air. The XPS data indicate that zinc sputtering, among the four tested metals, most affects the graphene as seen by the broadening of the main C1s signal. Interestingly, GO samples sputter-coated with metals behave somewhat differently than do CVD graphene samples, but both form similar materials characterized by defective carbon layers with a significant content of carbonyl groups; the results of those experiments are in (8) and fig. S3.

Sputtering damages graphene but does not remove it. Dissolving the zinc in acid is an essential step in removing the carbon layer. To investigate the role of the dissolving agent, we treated sputtered metals with different solutions. It was found that the carbon layer was removed when dissolving sputtered zinc using HCl or when dissolving sputtered aluminum using either HCl or concentrated NaOH. In all of those mixtures, H₂ gas is evolved. Conversely, no carbon layer was removed when dissolving sputtered copper in HCl/CuCl₂ or when dissolving sputtered gold in KI/I₂; no gas is evolved in those metal dissolutions. Although gas evolution probably plays a role in the carbon layer removal, a further difference of the two carbon-stripping metals, zinc and aluminum, versus the non-carbon-stripping metals, copper and gold, is in

their oxidation potentials. The combination of top-layer hole formation in the graphene, the large oxidation potentials of zinc and aluminum, as well as the evolved gas during their dissolution, all likely contribute to the mechanistic efficacy of the process.

The resolution that should be obtainable from this technique is being primarily dictated by the resolution of the metal patterning method. A 100-nm-wide zinc line was formed atop graphene with e-beam lithography, and a commensurately sized removal of the carbon layer was afforded by treatment with HCl (fig. S4). Furthermore, on the basis of AFM data, no delamination of the fabricated pattern corners or edges was observed while removing carbon layers from GO or HOPG. Over larger areas, scrolling of the edges was never observed by SEM.

We have demonstrated layer-by-layer removal of carbon from four types of graphene. This work demonstrates single-atomic-layer lithography in multilayer graphene structures and could provide impetus for the design of new graphene device embodiments.

References and Notes

1. A. K. Geim, K. S. Novoselov, *Nat. Mater.* **6**, 183 (2007).
2. K. S. Novoselov *et al.*, *Science* **306**, 666 (2004).
3. K. S. Novoselov *et al.*, *Nat. Phys.* **2**, 177 (2006).
4. G. Lu *et al.*, *Langmuir* **26**, 6164 (2010).
5. L. C. Campos, V. R. Manfrinato, J. D. Sanchez-Yamagishi, J. Kong, P. Jarillo-Herrero, *Nano Lett.* **9**, 2600 (2009).
6. L. B. Gao *et al.*, *J. Am. Chem. Soc.* **131**, 13934 (2009).
7. S. S. Datta, D. R. Strachan, S. M. Khamis, A. T. C. Johnson, *Nano Lett.* **8**, 1912 (2008).
8. Materials and methods are available as supporting material on Science Online.

9. W. S. Hummers, R. E. Offeman, *J. Am. Chem. Soc.* **80**, 1339 (1958).
10. D. C. Marcano *et al.*, *ACS Nano* **4**, 4806 (2010).
11. N. I. Kovtyukhova *et al.*, *Chem. Mater.* **11**, 771 (1999).
12. S. Stankovich *et al.*, *Carbon* **45**, 1558 (2007).
13. C. Gómez-Navarro *et al.*, *Nano Lett.* **7**, 3499 (2007).
14. V. C. Tung, M. J. Allen, Y. Yang, R. B. Kaner, *Nat. Nanotechnol.* **4**, 25 (2009).
15. C. Mattevi *et al.*, *Adv. Funct. Mater.* **19**, 2577 (2009).
16. X. Li *et al.*, *Science* **324**, 1312 (2009); 10.1126/science.1171245.
17. A. C. Ferrari *et al.*, *Phys. Rev. Lett.* **97**, 187401 (2006).
18. A. C. Ferrari, *Solid State Commun.* **143**, 47 (2007).
19. P. Lespade, A. Marchand, M. Couzi, F. Cruege, *Carbon* **22**, 375 (1984).
20. P. Poncharal, A. Ayari, T. Michel, J.-L. Sauvajol, *Phys. Rev. B* **78**, 113407 (2008).
21. Y. Hao *et al.*, *Small* **6**, 195 (2010).
22. S. Unarunotai *et al.*, *ACS Nano* **4**, 5591 (2010).
23. J.-H. Chen *et al.*, *Solid State Commun.* **149**, 1080 (2009).
24. K. Wasa, S. Hayakawa, *Handbook of Sputter Deposition Technology: Principles, Technology, and Applications* (Noyes, Park Ridge, NJ, 1991).
25. J. R. Hahn, H. Kang, S. Song, I. C. Jeon, *Phys. Rev. B* **53**, R1725 (1996).
26. J. R. Hahn, H. Kang, *Phys. Rev. B* **60**, 6007 (1999).
27. F. Banhart, J. Kotakoski, A. V. Krasheninnikov, *ACS Nano* **5**, 26 (2011).
28. F. Banhart, *Rep. Prog. Phys.* **62**, 1181 (1999).
29. G. L. Montet, G. E. Myers, *Carbon* **9**, 179 (1971).
30. D. Marton, K. J. Boyd, T. Lytle, J. W. Rabalais, *Phys. Rev. B* **48**, 6757 (1993).
31. M. Szymoński, *Appl. Phys. (Berl.)* **23**, 89 (1980).
32. F. Larachi, S. Dehkissia, A. Adnot, E. Chornet, *Energy Fuels* **18**, 1744 (2004).

Supporting Online Material

www.sciencemag.org/cgi/content/full/331/6021/1168/DC1
Materials and Methods
Figs. S1 to S4

18 October 2010; accepted 31 January 2011
10.1126/science.1199183

Helix-Rod Host-Guest Complexes with Shuttling Rates Much Faster than Disassembly

Quan Gan,^{1,2,3} Yann Ferrand,² Chunyan Bao,² Brice Kauffmann,² Axelle Grélard,² Hua Jiang,^{1*} Ivan Huc^{2*}

Dynamic assembly is a powerful fabrication method of complex, functionally diverse molecular architectures, but its use in synthetic nanomachines has been hampered by the difficulty of avoiding reversible attachments that result in the premature breaking apart of loosely held moving parts. We show that molecular motion can be controlled in dynamically assembled systems through segregation of the disassembly process and internal translation to time scales that differ by four orders of magnitude. Helical molecular tapes were designed to slowly wind around rod-like guests and then to rapidly slide along them. The winding process requires helix unfolding and refolding, as well as a strict match between helix length and anchor points on the rods. This modular design and dynamic assembly open up promising capabilities in molecular machinery.

Controlling motion at the molecular scale is key to the engineering of synthetic nanomachines (1–7). Such control can be exerted upon introducing irreversible bonding between different moving parts of a molecular structure so that motion only takes place in defined directions. In rotaxanes (8–11), rings are irreversibly locked

around rods along which they may slide. In catenanes (12), interlocked rings may rotate around one another. An important improvement to these designs would entail not forbidding undesired motions but rather segregating them to much longer time scales, just as biological molecular machines self-assemble and disassemble slowly while their work

regime is rapid (13). We now have implemented this concept in molecular shuttles that slowly bind to rods and then rapidly slide along them without requiring an irreversible attachment. The shuttles consist of oligomeric aromatic amide molecular tapes that fold into very stable helices possessing a cylindrical cavity with high affinities for complementary rod-like guests. A guest terminated with bulky ends cannot thread itself in the cavity but nevertheless forms a complex via a slow helix unfolding-refolding process, thereby allowing the helix to rapidly shuttle along the guest without dissociating.

Aromatic oligoamides **1**, **2**, and **3** (Fig. 1A) were designed according to well-established rules (14, 15) to fold into helical structures stabilized by local preferential conformations at aryl-amide linkages and intramolecular π - π interactions between aromatic groups (fig. S1) (16). Based on studies of

¹Beijing National Laboratory for Molecular Sciences, CAS Key Laboratory of Photochemistry, Institute of Chemistry, Chinese Academy of Sciences, Beijing, 100190, China. ²Institut Européen de Chimie et Biologie, Université de Bordeaux-CNRS UMR5248 and UMS3033, 2 rue Robert Escarpit, F-33607 Pessac, France. ³Graduate School of Chinese Academy of Sciences, Beijing, 100049, China.

*To whom correspondence should be addressed. E-mail: hjiang@iccas.ac.cn (H.J.); i.huc@iecb.u-bordeaux.fr (I.H.)

related compounds (17, 18), we predicted that the fluoroaromatic units in the center of the sequence would form a helix wide enough to accommodate an alkyl chain but nothing much larger, with each peripheral 2,6-pyridinedicarboxamide unit acting as a hydrogen bond donor to anchor the guest at a defined position in the helix cavity. Increasing strand length (from 3 to 1) adjusts the distance between the anchor points along the helix axis and their relative orientation in a plane perpendicular to the helix axis. It also tunes the time scale of helix unfolding and refolding dynamics, which may range from fractions of a second to minutes, hours, and even days for multi-turn helices, as demonstrated for helical quinoline-carboxamide oligomers (19).

Like other aromatic amide oligomers, compounds 1 to 3 fold into single-helical conformers, which then aggregate to form double-helical duplexes (Fig. 1C) (15, 16, 20). The structures of

the double helices (2)₂ and (3)₂ have been characterized in the solid state by x-ray crystallography (Fig. 2, A and B). Crystals of (1)₂ were also obtained, but their structure could not be solved due to very large unit cell parameters and poor diffraction intensity. In solution, the double helices prevail, and no signal of the single helices can be detected at equilibrium at 25°C by nuclear magnetic resonance (NMR) spectroscopy, even at low concentration. However, heating to 80°C in C₂D₂Cl₄ causes some duplex dissociation. The proportion of single helix is the same whether the sample is brought to 80°C by heating or by cooling, indicating that equilibrium is reached rapidly at this temperature (20). Under these conditions, integration of the single and double helix signals gives a measure of dimerization constants at 80°C: 2.8 × 10⁵, 6.4 × 10⁵, and >10⁶ liter mol⁻¹ for 1, 2, and 3, respectively.

Anticipating the need to match helix length with guest length, we prepared a range of rod-

shaped guests, 4a to 4g, incorporating a successive number of methylene units. We then treated each in turn with 1, 2, or 3 in CDCl₃ solutions and monitored changes by ¹H NMR (nuclear magnetic resonance). In some cases, the signals of the duplexes disappeared, and a new species emerged corresponding to a complex in which a single helix is wound around a rod-shaped guest (Fig. 1, C and D to G). Because the kinetics of host-guest complex formation can be extremely slow at room temperature (see below), all titrations were carried out at 45°C and binding constants calculated at that temperature (Fig. 1H). A guest with no stopper was prepared (5) to assess the mechanism of complex formation. Guests with 4,4-diphenyl-butyl stoppers (e.g., 6 and 7) are more soluble and less prone to crystallize on their own than those with benzyl stoppers and proved to be more suitable for the crystallographic analysis of the complexes.

The stoichiometry and structure of the host-guest complexes were assessed in the solid state (Fig. 2), in solution, and in the gas phase. In solution, multiple intermolecular nuclear Overhauser effect (NOE) correlations were observed between aromatic amide protons of the helices and aliphatic alkyl protons of the guests (fig. S18); some of the guests' protons became diastereotopic in complexes due to the chiral environment of the helix (Fig. 1G); aromatic signals of the complexes are shifted downfield from those of the double helices, indicating weaker ring current effects and thus less extensive π-stacking as expected in the single helix (Fig. 1, D to G). Diffusion-ordered spectroscopy (21) showed that the diffusion coefficient of the complex is similar to (slightly higher than) that of the double helix (fig. S19). Both titration data in solution and mass spectrometry in gas phase confirmed that the complexes consist of a monomeric helix and one equivalent of guest (fig. S24). Crystallographic data confirmed the structure in the solid state and showed that the 2,6-pyridinedicarboxamide units of the helices hydrogen bond to the carbonyl groups of the guests (fig. S25). It follows that the complexes form only when the helix and the guest match in length with a tolerance of at most one CH₂ unit of the guest (Fig. 1H). Helices longer than 1 are expected to bind selectively to longer guests, demonstrating a high modularity in space of this system. The affinity of the single helices for their guests is clearly high enough to overcome their strong propensity to form double helices. This is facilitated by the fact that it takes two strands to form a duplex and only one to form a host-guest complex: The helix dimerization constant is in balance with the square of the rod-helix association constant.

The host-guest complexes between the shortest oligomers 2 and 3 and their respective guests form readily at 25°C. However, complexes involving 1 do not form even after days unless the mixture undergoes a heating-cooling cycle. The reasons lie in slow kinetics of complex formation from the single helix and in very slow kinetics of double helix dissociation into single helices (20). The pure single-helical conformer of 1 could be fortuitously

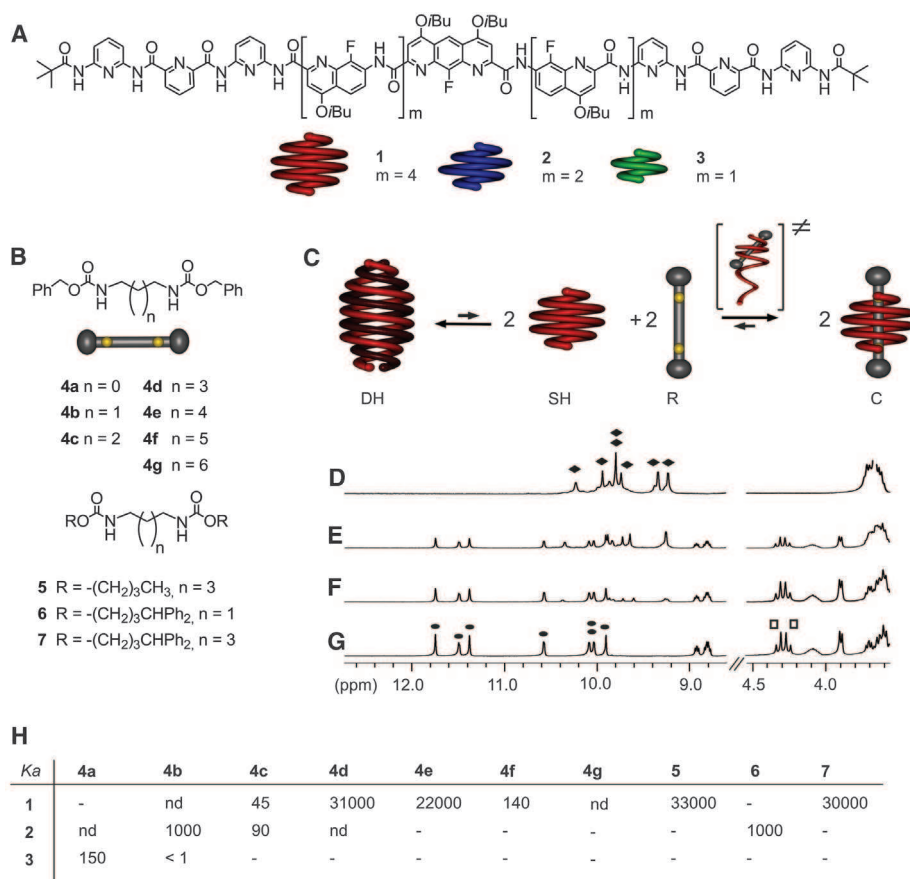


Fig. 1. Host-guest components and assembly. (A) Formulas of 1, 2, and 3. Single-helical conformations span 4.5, 3.5, and 2.5 turns, respectively. (B) Rod-like guests possessing carbonyl hydrogen bond acceptors (yellow dots) with bulky end groups (4, 6, 7) or without (5). Depending on length (*n*), each guest matches best with 1, 2, or 3 as a host. (C) Equilibrium between oligomers 1, 2, and 3 as double helices (DH), single helices (SH), or complexes (C) with rod-like guests (R). The formation of a complex with a dumbbell guest requires the unfolding and refolding of the helix. (D to G) Titration of 1 (2 mM) by 4d [from (D) to (G): 0, 0.5, 1, 1.5 equiv. of 4d] monitored by 400-MHz ¹H NMR in CDCl₃ at 45°C. The high temperature reduces the time needed to reach equilibrium after each addition of 4d. The signals of the starting double helix (1)₂ (♦) progressively disappear while the signals of 1>4d emerge (●). Benzylic protons of the bound 4d appear as a diastereotopic pattern (□), which reflects the chiral environment of the surrounding helix. (H) Constants of formation at 45°C of the complexes between 1 to 3 and 4 to 7 defined as *K_a* = [C]²/([DH]·[R]²). nd: no binding detected.

isolated by selective precipitation from methanol even though it constitutes a minor component in solution. Upon dissolving it again in CDCl_3 , the double helix slowly forms over 24 hours at 2 mM if no guest is present (fig. S4). However, in the

presence of **7**, which possesses very bulky end groups, the complex **1**⋯**7** forms at 25°C over the course of 30 min, which allowed us to estimate a kinetic constant of dissociation slower than 2 day^{-1} (fig. S21). In contrast, **5** does not possess any bulky

group and forms a complex **1**⋯**5** at rates too fast to monitor. These results indicate that complexes such as **1**⋯**5** may form by a simple threading of the guest into the helix cavity, whereas the formation of **1**⋯**7** requires an unwinding and rewinding of the helix around the guest (Fig. 1C) (22–24). The crystal structures of **1**⋯**7** and **1**⋯**5** shown in Fig. 2, D and E, illustrate that **5** is thin enough to thread itself into the helix of **1** whereas **7** is much too bulky to do so. These complexes relate to some structurally labile rotaxane structures in which molecular rings are closed by noncovalent bonds (25, 26) or by reversible covalent attachments (27, 28).

High host-guest stability and slow formation kinetics in the case of **1**⋯guest hint at even slower kinetics of complex dissociation. Indeed, complexes such as **1**⋯**7** can be eluted on a silica thin-layer chromatography plate without any observable dissociation (fig. S22). We thus endeavored to explore the extent to which helices of **1** wrapped around guests could undergo sliding motions more rapidly than they dissociate. Rod-like guest **8** possesses three hydrogen bond acceptors and thus two degenerate stations, which, because of their proximity, can bind only one helix at a time (Fig. 3A). Both solution and solid-state (Fig. 2F) data confirm that **8** forms a 1:1 complex with oligomer **1**. The rate of formation of **1**⋯**8** is almost identical to that of **1**⋯**7** (figs. S20 and S21). The single helix of **1** is C_2 symmetrical, but this symmetry is broken in **1**⋯**8** because one extremity of **1** lies near the central urea function of **8** whereas the other extremity is bound to one of the two carbamate functions. This loss of symmetry is seen in the ^1H and ^{19}F NMR spectra of **1**⋯**8**, which feature twice as many signals as symmetrical complexes. The two extremities of **1** should exchange their environments when **1** goes from one binding station of **8** to the other (Fig. 3B). Exchange spectroscopy NMR (29) experiments were carried out on solutions of **1**⋯**8** and showed clear correlation resulting from the motion of **1** between the two stations of **8**. This motion can be calculated to take place at rates between 2 and 4 min^{-1} at 25°C, a time scale considerably smaller than that of host-guest complex dissociation, implying that **1** exchanges between the two stations of **8** via a sliding (shuttling) process and not via a dissociation (unfolding)–association (refolding) mechanism.

A step beyond random sliding consists in triggering motion so that all molecules in an ensemble undergo the same change within a given time window. To reach this objective, we designed guest **9** with two different binding stations: one with a heptyl segment, the other with a diethylamine segment, with the expectation that a host-guest complex would form on the neutral amine segment but not on the corresponding ammonium. As with **8**, only a 1:1 complex forms between **1** and **9**, as confirmed by integrating the ^1H NMR signals belonging to **1** and to **9** in **1**⋯**9**. However, **1** may not reside equally at the two different stations of **9**. Indeed, ^1H and ^{19}F NMR spectra of **1**⋯**9** feature two sets of signals in slightly different

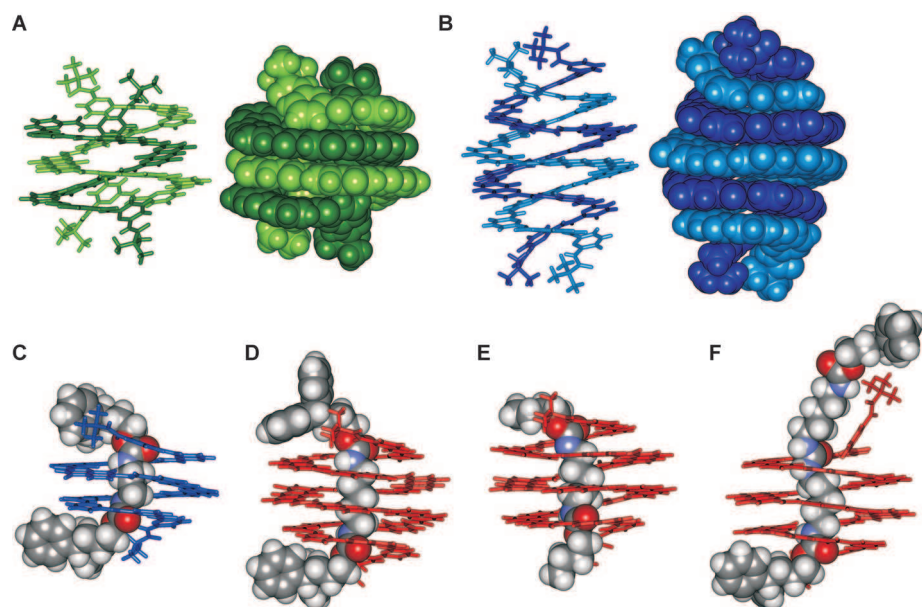


Fig. 2. Solid-state structures. (A) Double helix (**3**)₂. (B) Double helix (**2**)₂. (C) Complex **2**⋯**6**. (D) Complex **1**⋯**7**. (E) Complex **1**⋯**5**. (F) Complex **1**⋯**8**. Side chains (O-isobutyl groups) and included solvent molecules have been removed for clarity.

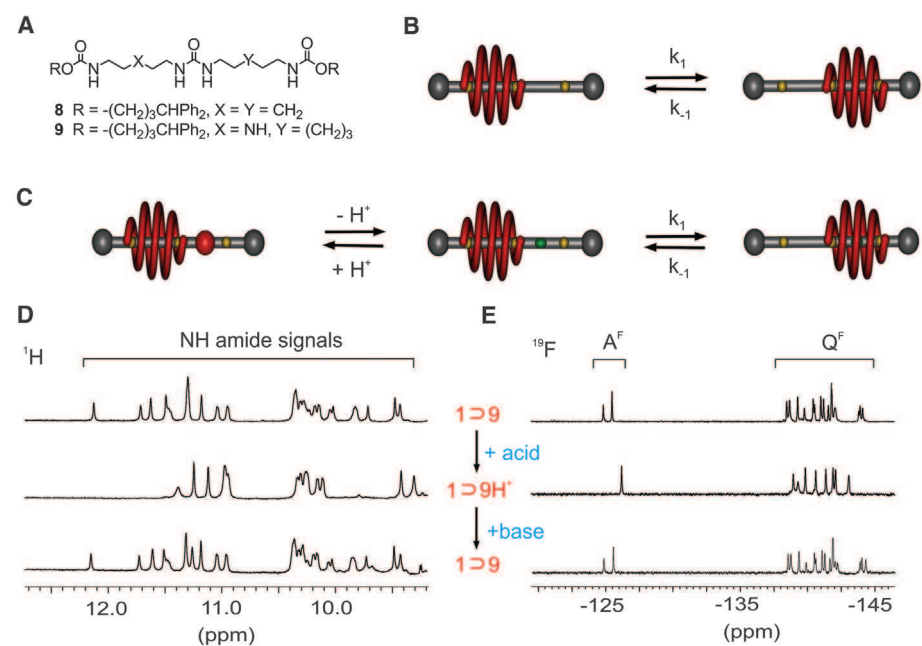


Fig. 3. Helix shuttling. (A) Formulas of rod-like guests having two adjacent identical (**8**) or different (**9**) stations. Because of the proximity between the two stations and the presence of a single carbonyl group in the middle of the rod, only one station at a time can be occupied by a helix. (B) Scheme of degenerate helix sliding along a symmetrical guest. The yellow dots mark the hydrogen bond acceptors. (C) Scheme of helix sliding along a nondegenerate guest possessing a station that can be blocked or unblocked upon protonation or deprotonation, respectively. The green dot symbolizes the amine function of **9**, which can be included in the helix cavity. The red dot is the corresponding ammonium, which is not included in the helix cavity. (D and E) Portions of the ^1H and ^{19}F NMR spectra of **1**⋯**9** in CDCl_3 at equilibrium, after adding excess of an organic acid (2,4-dinitrophenol) and after neutralizing with a base (Et_3N). A^{F} and Q^{F} designate fluoro-anthracene and fluoro-quinoline, respectively.

(58/42) proportions corresponding to a slight bias in favor of one station. Upon titrating **1** with an acid, the smaller NMR signals disappear without any measurable delay during the measurement of a ^1H NMR spectrum (~ 2 min), and only one set of signals remains after adding excess acid (Fig. 3, D and E). This is consistent with the trapping of **1** on a single station of **9**, as it is repelled by the ammonium function of the other station. Adding a base instantly reverses the process. Again, the time scale of this controlled motion is much faster than the rates of unfolding and refolding of **1** around **9**, implying that motion is mediated by the rapid sliding of **1** along **9**.

Using helices longer than **1** should expectedly result in slower sliding but also in much slower helix-rod dissociation. Combining rods with multiple distinct stations with mixtures of helices of different lengths should thus allow several controlled motions to proceed at different rates within a single supramolecular construct.

References and Notes

- W. R. Browne, B. L. Feringa, *Nat. Nanotechnol.* **1**, 25 (2006).
- C. Mao, W. Sun, Z. Shen, N. C. Seeman, *Nature* **397**, 144 (1999).
- T. R. Kelly, H. De Silva, R. A. Silva, *Nature* **401**, 150 (1999).
- S. P. Fletcher, F. Dumur, M. M. Pollard, B. L. Feringa, *Science* **310**, 80 (2005).
- T. Muraoka, K. Kinbara, T. Aida, *Nature* **440**, 512 (2006).
- K. Miwa, Y. Furusho, E. Yashima, *Nat. Chem.* **2**, 444 (2010).
- S. Hiraoka, E. Okuno, T. Tanaka, M. Shiro, M. Shionoya, *J. Am. Chem. Soc.* **130**, 9089 (2008).
- J. D. Badjic, V. Balzani, A. Credi, S. Silvi, J. F. Stoddart, *Science* **303**, 1845 (2004).
- J. E. Green *et al.*, *Nature* **445**, 414 (2007).
- V. Serreli, C.-F. Lee, E. R. Kay, D. A. Leigh, *Nature* **445**, 523 (2007).
- M. R. Panman *et al.*, *Science* **328**, 1255 (2010).
- P. Mobian, J.-M. Kern, J.-P. Sauvage, *Angew. Chem. Int. Ed.* **43**, 2392 (2004).
- K. Kinbara, T. Aida, *Chem. Rev.* **105**, 1377 (2005).
- I. Huc, *Eur. J. Org. Chem.* **2004**, 17 (2004).
- V. Berl, I. Huc, R. G. Khoury, M. J. Krische, J.-M. Lehn, *Nature* **407**, 720 (2000).
- Materials and methods are detailed in supporting material at Science Online.
- E. Berni *et al.*, *Chem. Commun. (Camb.)* **2008** (no. 17), 1968 (2008).
- C. Bao *et al.*, *Angew. Chem. Int. Ed.* **47**, 4153 (2008).
- N. Delsuc *et al.*, *ChemPhysChem* **9**, 1882 (2008).
- B. Baptiste *et al.*, *Chem. Asian J.* **5**, 1364 (2010).
- Y. Cohen, L. Avram, L. Frish, *Angew. Chem. Int. Ed.* **44**, 520 (2005).
- T. Nishinaga, A. Tanatani, K. Oh, J. S. Moore, *J. Am. Chem. Soc.* **124**, 5934 (2002).
- A. Tanatani, T. S. Hughes, J. S. Moore, *Angew. Chem. Int. Ed.* **41**, 325 (2002).
- A. Petitjean, L. A. Cuccia, M. Schmutz, J.-M. Lehn, *J. Org. Chem.* **73**, 2481 (2008).
- C. A. Hunter *et al.*, *Angew. Chem. Int. Ed.* **40**, 2678 (2001).
- S.-Y. Chang, H.-Y. Jang, K.-S. Jeong, *Chemistry* **9**, 1535 (2003).
- P. T. Glink, A. I. Oliva, J. Stoddart, A. J. P. White, D. J. Williams, *Angew. Chem. Int. Ed.* **40**, 1870 (2001).
- M. Horn, J. Ihringer, P. T. Glink, J. F. Stoddart, *Chemistry* **9**, 4046 (2003).
- C. L. Perrin, T. J. Dwyer, *Chem. Rev.* **90**, 935 (1990).
- This work was supported by the CNRS, the Conseil Régional d'Aquitaine, the Chinese Academy of Sciences, and the National Natural Science Foundation of China (20772127, 20972164). We thank C. Müller-Dieckmann for beamtime and help during data collection on ID29 at the European Synchrotron Radiation Facility. Crystallographic data for (**3**)₂, (**2**)₂, **2**⋅**6**, **1**⋅**7**, **1**⋅**5**, and **1**⋅**8** have been deposited with the Cambridge Crystallographic Data Centre under reference numbers CCDC-797906, 797911, 797907, 797908, 797910, and 797909, respectively.

Supporting Online Material

www.sciencemag.org/cgi/content/full/331/6021/1172/DC1
Materials and Methods
Figs. S1 to S31
Tables S1 to S9
References

8 November 2010; accepted 20 January 2011
10.1126/science.1200143

Oxygen Isotope Variations at the Margin of a CAI Records Circulation Within the Solar Nebula

Justin I. Simon,^{1,2*} Ian D. Hutcheon,³ Steven B. Simon,⁴ Jennifer E. P. Matzel,³ Erick C. Ramon,³ Peter K. Weber,³ Lawrence Grossman,⁴ Donald J. DePaolo²

Micrometer-scale analyses of a calcium-, aluminum-rich inclusion (CAI) and the characteristic mineral bands mantling the CAI reveal that the outer parts of this primitive object have a large range of oxygen isotope compositions. The variations are systematic; the relative abundance of ^{16}O first decreases toward the CAI margin, approaching a planetary-like isotopic composition, then shifts to extremely ^{16}O -rich compositions through the surrounding rim. The variability implies that CAIs probably formed from several oxygen reservoirs. The observations support early and short-lived fluctuations of the environment in which CAIs formed, either because of transport of the CAIs themselves to distinct regions of the solar nebula or because of varying gas composition near the proto-Sun.

Calcium-, aluminum-rich inclusions (CAIs) are understood to have formed very early in the evolution of the solar system and in contact with nebular gas, either as solid condensates or as molten droplets. In general, CAIs are ^{16}O -rich relative to planetary materials and are believed to record the $\Delta^{17}\text{O}$ (I) composition of solar nebular gas in which they grew (2). $\Delta^{17}\text{O}$ may be a marker of radial position within the solar nebula. Less prim-

itive nebular materials (such as iron-, magnesium-rich chondrules) typically have planetary-like values ($\Delta^{17}\text{O} = 0$) and may have formed further out in the protoplanetary disk from where CAIs formed (3). Previous oxygen isotopic studies document substantial variation in the $\Delta^{17}\text{O}$ of CAIs (2, 4), but because of their lower spatial resolution ($\geq 10\ \mu\text{m}$) have not been able to probe the isotopic stratigraphy of the outer parts of CAIs with enough resolution to detect the continuous range of isotopic variations observed here. Because models suggest that radial transport of primitive matter may have played an important role in the evolution of protoplanetary disks (5–7), evidence within individual CAIs for transfer among distinct regions in the solar nebula, such as systematic $\Delta^{17}\text{O}$ variations, is of critical importance.

To further investigate intra-CAI oxygen isotopic variations, a component of the CV3 carbonaceous chondrite Allende (the CAI called A37), its surrounding concentric rim, and a micro-CAI enclosed within this rim were measured with NanoSIMS, an ion microprobe with nanometer-scale spatial resolution. Measurements were obtained as $\sim 2\text{-}\mu\text{m}$ spot analyses spaced every 7 to 10 μm across the rim and the outer $\sim 150\ \mu\text{m}$ of the interior (Fig. 1) (8). At the resolution that is accessible with NanoSIMS, both A37 and its rim exhibit more than 20 per mil (‰) variation in $\Delta^{17}\text{O}$, a range that is close to the full range thought to exist among solids formed in the solar system. Mass-dependent physicochemical processes cannot produce variations in $\Delta^{17}\text{O}$. These data imply that A37 was transported among several different nebular oxygen isotopic reservoirs (4), potentially as it passed through and/or into various regions of the protoplanetary disk.

Concentric multi-mineralic rim sequences [so-called Wark-Lovering (WL) rims (9)] are a widespread feature that indicates that many CAIs shared a similar evolution history to each other and possibly to less primitive materials, despite the compositional and mineralogical diversity of their interiors. These ubiquitous WL rims formed late—although still relatively early in solar system history according to evidence that they initially contained a canonical abundance of the short-lived nuclide ^{26}Al (10). The preservation of their primitive age attests to the fact that they have experienced minimal subsequent disturbance either in the nebula or on the chondrite parent body. The mineralogy and composition of the WL rims surrounding CAIs suggest that late in their evolution, the CAIs were in a nebular environment distinct from that where they origi-

¹Astromaterials Research Office KR111, NASA Johnson Space Center, Houston, TX 77058, USA. ²Center for Isotope Geochemistry, University of California, Berkeley, Berkeley, CA 94720, USA. ³Lawrence Livermore National Laboratory (LLNL), Livermore, CA 94551, USA. ⁴Department of Geophysical Sciences, University of Chicago, Chicago, IL 60637, USA.

*To whom correspondence should be addressed. E-mail: justin.i.simon@nasa.gov